The Acetylene Bending Spectrum at $\sim$10000 cm^{-1}: Quantum Assignments in the Midst of Classical Chaos

Christof Jung

Centro de Ciencias Fisicas, UNAM, Av. Universidad s/n, 62251 Cuernavaca, Mexico

Howard S. Taylor*

University of Southern California, Los Angeles, California 90089-0482

Matthew P. Jacobson

Physical and Theoretical Chemistry Laboratory, South Parks Road, Oxford OX1 3QZ, U.K.

A combination of quantum mechanics, semiclassical mechanics, and nonlinear classical dynamics is used to extract the detailed internal molecular motions that underly the quantum eigenstates of acetylene with 16 quanta of total bend excitation. No potential energy surface is used; rather, the states are represented by an algebraic effective Hamiltonian that has been extensively refined against experimental data. The classical mechanical analysis reveals widespread chaos, but the quantum mechanical structure is surprisingly regular. Specifically, all 81 quantum states can be assigned a pair of semiclassical quantum numbers that reveal the underlying classical motions associated with each state. These classical motions range continuously between limiting-case motions that we refer to as local bend (one hydrogen bending) and counter-rotation (the two hydrogens undergoing circular motions in planes perpendicular to the CC axis). The first reason that the regularity in the quantum structure was previously undetected is that the identification of regular nodal coordinates, if any exist, of quantum wave functions in a multidimensional (i.e., greater than two dimensions) space is generally a difficult task; our success here was made possible by the identification in a reduced two-dimensional (2D) space of two families of periodic orbits (dynamic modes) which evolve with energy. Every quantum state reflects the quantization of the two dynamic mode system. The second reason for the undetected regularity is that the regular sequences of quantum levels that we have identified are interspersed among each other in energy, thus giving the appearance of a complex, unassignable spectrum.

1. Introduction

The bending dynamics of acetylene have been subjected to intense scrutiny in the past 10 years in a series of experimental and theoretical studies.[1−14] In a number of these studies, it has been noted that the acetylene bending dynamics is particularly complicated at roughly 10 000 cm^{-1} of bend excitation. In the early work of Jonas and co-workers,[2] which made the first steps toward interpreting the complex stimulated emission pumping and dispersed fluorescence spectra of acetylene, it was noted that the ability to fit a Dunham expansion to the observed sequence of (trans) bending states fundamentally broke down at 14−16 quanta of excitation, which corresponds to $\sim$10 000 cm^{-1} of vibrational energy. They attributed this breakdown to the onset of rapid intramolecular vibrational energy flow, specifically due to a Darling-Dennison bend resonance. Subsequent work has refined this understanding of the mechanisms of vibrational energy flow, and a spectroscopic effective Hamiltonian has been developed that reproduces all relevant experimental data up to 15 000 cm^{-1} with 1.5 cm^{-1} precision.[1,8,11]

However, the ability to fit data to an appropriate model should not be confused with an understanding of the molecular dynamics. To this end, a number of theoretical studies have appeared which have analyzed models of acetylene bending dynamics using quantum, semiclassical, and/or classical mechanics,[5,7,11−13] and each of these has noted that the dynamics is quite complicated near 10 000 cm^{-1} of bend excitation. The observations that have led to this conclusion have included a complex eigenstate level structure and associated complicated quantum wave packet dynamics;[11] complex classical mechanics, with new classes of periodic orbits being born and classical chaos increasing in prominence;[5,7,12,13] and of particular significance to this paper, the inability to assign conventional spectroscopic quantum numbers (either normal mode or local mode) to many of the bending eigenstates with 14−16 quanta of excitation.[7,11]

The fundamental reason for the complex dynamics with around 10 000 cm^{-1} of bend excitation, as has been sketched out previously[2,7,11,13] and will be elaborated upon below, is that, by this energy, the effective trans and cis bend frequencies have become nearly equal. That is, the low-energy dynamics are dominated by the normal modes of vibration, in the sense that the vibrational Hamiltonian is approximately separable in the normal modes at low energy. However, when the trans and cis bend frequencies become nearly degenerate, which occurs at roughly 12 quanta of excitation, they become unstable and the anharmonic couplings begin to dominate the dynamics. As a result, the dynamics of the system change radically, although not all at once. Chaos gradually increases in prominence, and

new classes of stable and unstable classical periodic orbit motions emerge.

In a previous study of acetylene bending dynamics,[13] which focused on the semiclassical assignment of bending states with 22 quanta of total bend excitation, we performed a preliminary analysis of the evolution of the classical bending dynamics of acetylene with bend excitation, and determined that classical chaos was maximally prominent at $\sim$10 000 cm^{-1} of bend excitation (16 quanta). Our expectation was that this energy regime might be a good one for investigating possible quantum signatures of classical chaos (such studies abound in the literature but those that focus on real molecular systems, as opposed to model systems, are relatively rare). This expectation, however, was not fulfilled. Instead, the major, surprising conclusion of this work is that, despite the dominance of chaos in the classical dynamics, *all* of the bending eigenstates of acetylene with a total of 16 quanta of bend excitation can be assigned semiclassical quantum numbers, which from the simplest viewpoint represent the number of nodes along two families of periodic orbits (which are unstable at many energies).

The success of the semiclassical assignment scheme implies that there exists a regularity in the quantum structure that was previously undetected and unsuspected. Why have we succeeded in assigning the eigenstates here, while they previously seemed to be intrinsically unassignable? The answer to this question is multifaceted, and we enumerate several key issues below:

1. Our semiclassical scheme assigns the eigenstates in terms of a dynamic set of coordinates defined by periodic orbits,[15] and is thus much more flexible than traditional assignments in terms of orthogonal coordinate systems, such as normal or local modes. Normal mode coordinates are of course guaranteed to be appropriate for making assignments at sufficiently low vibrational excitation, and local mode coordinates have led to assignments for many eigenstates at higher energies.[5,7,11] However, normal and local modes only represent limiting case behaviors for the nonlinear, nonintegrable vibrational dynamics, as has been emphasized in our previous study,[13] which revealed a rich variety of periodic motions near 15 000 cm^{-1} of bend excitation, many of which could not easily be categorized as normal or local mode motions.

2. Our approach exploits the existence of approximate constants of motions (polyad numbers) to reduce the dimensionality of the acetylene bending system from 4 (two doubly degenerate bends) to 2 degrees of freedom. The constants of motion are N_b, the total number of quanta of bend excitation, and l, the total vibrational angular momentum. The latter of these is rigorously conserved in the absence of Coriolis interactions, while the former is approximately conserved by the molecule (on a time scale of at least a few picoseconds[10]) and rigorously conserved by the model that we employ. The ability to study the dynamics in two dimensions makes possible the use of surfaces of section, to gain a complete, detailed overview of the classical mechanics, as well as direct visual comparison of periodic orbits and wave functions, to establish the assignments. The coordinates in the reduced two-dimensional (2D) space are rather abstract and do not have obvious physical meanings, although we can (approximately) reconstruct such meaning by a mathematical transformation that we call a "lift".

3. In retrospect, it is clear why the eigenstate spectrum appeared to be unassignable. The eigenstates are quantized along two families of periodic orbits, and the resulting progressions of quantum levels are interspersed in energy. In addition, the underlying periodic orbits evolve rapidly with energy; the associated variation of the frequencies of the periodic orbits implies that the energy level spacings of the quantum progressions are highly nonuniform.

4. Finally, although the classical dynamics is dominated by chaos, the regular quantum progressions exist because certain slightly unstable periodic orbits organize the quantum structure more effectively than we expected. At many energies within the $N_b = 16$ polyad, the classical phase space is almost totally chaotic, and the quantizing periodic orbits are unstable, although only slightly so, such that many trajectories when in the vicinity of these periodic orbits mimic their motion. The result is that the quantum mechanics "sees" near these periodic orbits regions of sufficient order and dynamic attraction[15] on the scale of $\hbar$ to give rise to "scarred" quantum states.[16]

Because our semiclassical assignment scheme is relatively easily understood without understanding the quantum, semi-classical, and nonlinear classical methodologies we used to uncover it; because these methodologies are discussed in ref 13 and similar methodologies are, individually and in various combinations, discussed in other published works,[5,7,12,17,18] and because many of the probable audience for this paper are not versed nor wish to be immersed in the details of all these methodologies, this paper will start with a simple, didactic overview of our results and how we obtained them. The relationship between our method of analysis and others reported in the literature will be also clarified. Details of our model and methodology will follow, along with detailed results for $N_b = 16$.

2. Overview of Semiclassical Assignments

Our assignment scheme is motivated by the classical periodic orbit structure that is associated with the pure bend polyad ($N_b = 16$, $l = 0$) which comprises all states with a total of 16 quanta of bend excitation and zero total vibrational angular momentum. As outlined in the vertical middle of Figure 1, the periodic orbits within this polyad can be organized into two families, which evolve as a function of energy, and merge at the energy extremes of the polyad. The periodic orbit motion at the very lowest energy within the polyad can be described as a pure "local bend" (one hydrogen bending, the other stationary) while the top of the polyad is associated with counter-rotation (both hydrogens undergoing circular motions in planes perpendicular to the CC axis, in opposite directions). The periodic motions at intermediate energies are more complicated and vary continuously between local bend and counter-rotation.

Our semiclassical scheme assigns a pair of quantum numbers, which we write generically as (n_1, n_2), to each eigenstate, according to its structure along the relevant periodic orbits from each family at the energy in question. In some cases, the quantum number assignments can be made using EBK quantization, which is possible only when tori (regions of regular classical dynamics that surround stable periodic orbits in phase space) exist; in this case, n comes from the loop integrals of those tori when the loop integrals are integer multiples of $\hbar$. For many states, EBK quantization is not possible, because classical chaos dominates in the middle of the polyad and the orbits are either unstable or only weakly stable (in the sense that they are surrounded by small torus bundles). Nonetheless, *all* of the eigenstates can be assigned semiclassically by visual inspection. In the case of librational states (restricted motion), the quantum number n represents a node count along the relevant periodic orbit, while for rotational states, n represents a phase advance along the orbit. Note that here "rotation" does not refer to a physical rotation of the molecule or the hydrogens, but rather to unrestricted motion in the abstract space of classical angles in which we perform our analysis; see below.
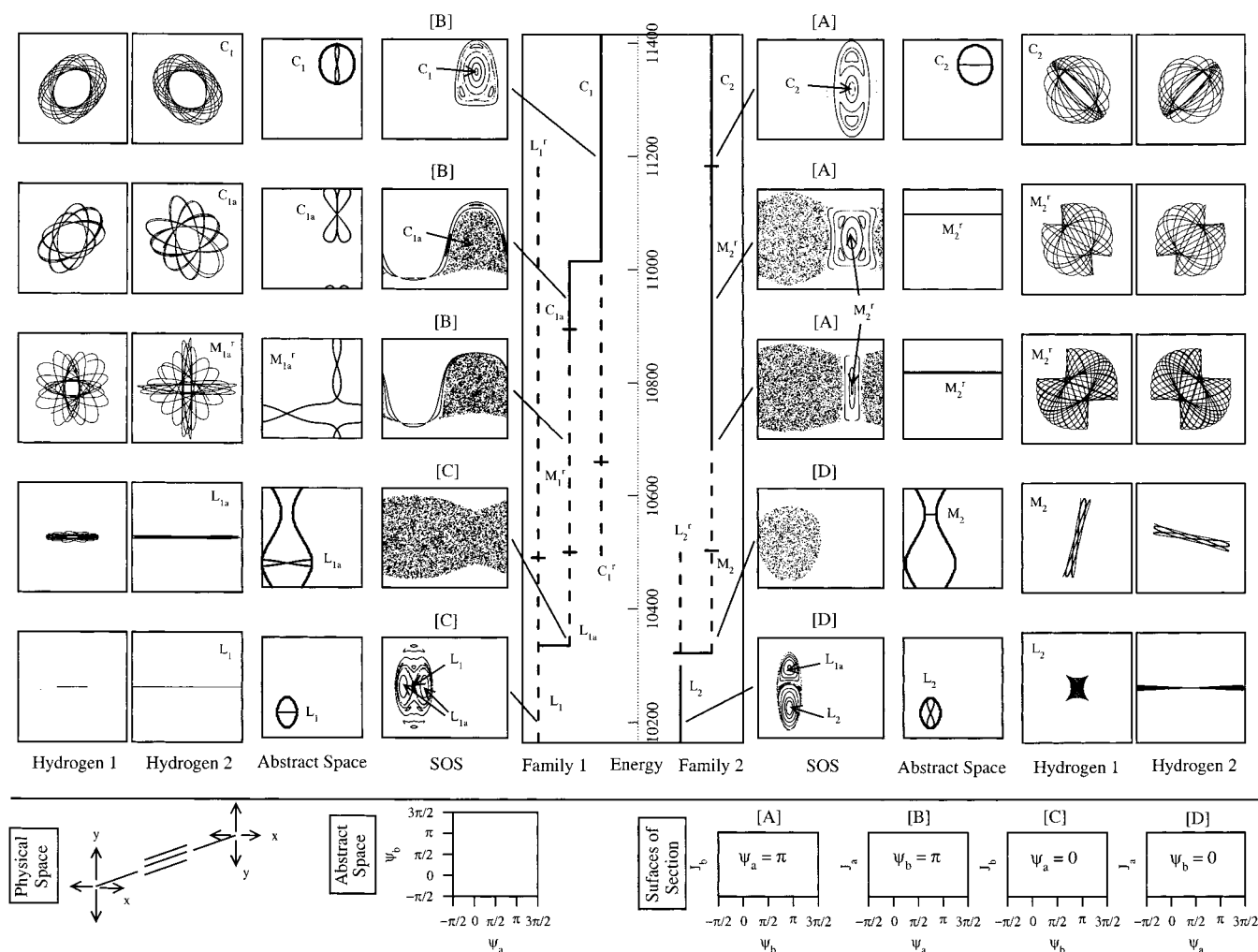
Figure 1. Summary of the classical mechanics in the $N_b = 16$, $l = 0$ polyad. Central column: Schematic overview of the periodic orbits within the polyad. The periodic orbits can be grouped into two "families", which connect smoothly from the highest to the lowest energy within the polyad. A solid line indicates a stable orbit, while a dashed line indicates an unstable orbit. Columns 4 and 6: Surfaces of section; the various coordinates for these plots, and the intersection conditions, are shown at the bottom of the diagram. Columns 3 and 7: Selected periodic orbits in the abstract space of classical angles, (ψ_a, ψ_b). Columns 1, 2, 8, and 9: Periodic orbit motions depicted as physical displacements of the hydrogens from the CC axis, as determined from the "lift" procedure.

Figures 2 and 3 summarize the semiclassical assignments. Ideally, these figures would be rotated by 45°, with the highest and lowest energy eigenstates at the top and bottom of the page, respectively. The states which are assigned as $(n_1, 0)$ and $(0, n_2)$ (excitation along only one of the families of periodic orbits) are on the outer edges of the diagram. Along both series of states, the underlying classical motion varies from local bend at the bottom to counter-rotation at the top, although the evolution of the dynamics occurs in different ways for each family. In Family 2, the motion that starts out as pure local bend gradually acquires increasing excitation in the second (initially stationary) hydrogen, in a plane perpendicular to the first. Eventually, the amplitude of the two bends becomes equal; quantum states associated with this "cross" bending motion are located in the upper left corner of Figures 2 and 3. From this point, the motion continues to evolve by gradually incorporating increasing rotational character, and thus increasingly resembling a perfect counter-rotation. In Family 1, the initial local bend motion evolves by once again acquiring increasing excitation in the second hydrogen, except this time primarily in the same plane as the first. The intermediate motions for Family 2 are somewhat more difficult to visualize than for Family 1, but the hydrogens tend to oscillate about some axis for a period of time before switching to an orthogonal axis.

Such "axis switching" states are located in the lower right corner of the figures.

Up to this point we have simply stated that we can assign a pair of quantum numbers to each eigenstate according to the number of quanta of excitation along the relevant Family 1 and 2 periodic orbits. Having organized the quantum states as in Figures 2 and 3, we could simply label states in particular sequences according to their energy rank. We choose instead to label the states using *quantum numbers whose values represent the level of quantum excitation along particular periodic orbit motions*. Because each Family is composed of several separate periodic orbits that are connected through bifurcations, the appropriate quantum labels change with energy. We have already suggested above that the classical dynamics are maximally simple at the energy extremes of the polyad, and thus the low- and high-lying states are labeled by two sets of numbers ($n_{L1/2}$ for local bend-like motions and $n_{C1/2}$ for counter-rotation) which increase toward the center of the polyad (upper left and lower right corners of the diagram). The multiple quantum assignments appearing at the top of the diagrams reflect the transitional nature of the phase space structures in the middle of the polyad between simpler structures (and associated motions) at lower and higher energies. As a result, the nodal coordinates of these eigenfunctions can be interpreted in
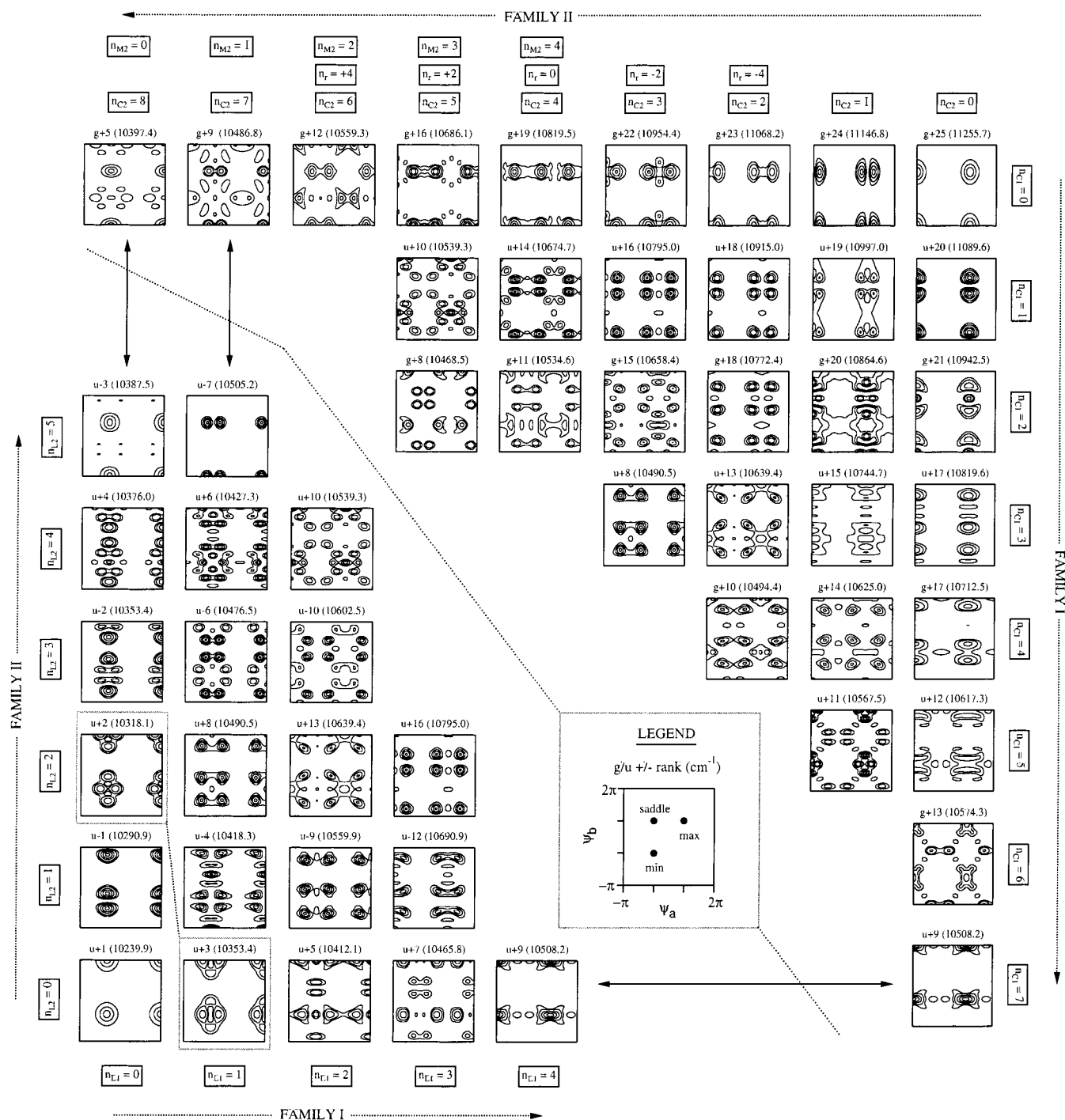
Figure 2. Semiclassical assignments for roughly half of the quantum eigenstates with $N_b = 16$ and $l = 0$. The lower left corner depicts those states that can be labeled with (n_{L1}, n_{L2}) quantum numbers, and with $u+$ and $u-$ symmetry. The upper right corner includes all states which can be labeled with (n_{C1}, n_{C2}) quantum numbers, and which have $g+$ or $u+$ symmetry. In some cases, the n_{M2} or n_r quantum numbers provide a more physically meaningful assignment than n_{C2}; see the text for details.

different ways, depending on whether they are viewed as progressing from low to high energy or vice versa. That is, the middle states admit multiple quantum state labels, although each state retains a single dynamical interpretation.

We have neglected to discuss several important details, such as the axes of the wave function plots, which are classical angles. We also note briefly that certain wave functions seem out of place in the figure, such as those connected by the dotted lines. These wave functions occur in accidental near degeneracies, and the more complicated nodal patterns are caused by interferences between the semiclassically "pure" states. With a little practice, it is usually possible to visually untangle the interfer-

ences. Interestingly such accidental degeneracies were also noted in ref 18 which like here used nonlinear dynamics and the classical quantum correspondence to help assign highly excited states in the water molecule. In ref 18 it was pointed out that these complicated wave functions could have been mistaken in the past for functions whose phase space transforms lie in a chaotic region of phase space.

With the above caveat in mind, we conclude that the assignment of each state in the polyad can be given in the sense that every state has as many quantum numbers (n_1, n_2, N_b, $l = 0$) as there are degrees of freedom, and that each state has a corresponding visualizable classical internal molecular motion
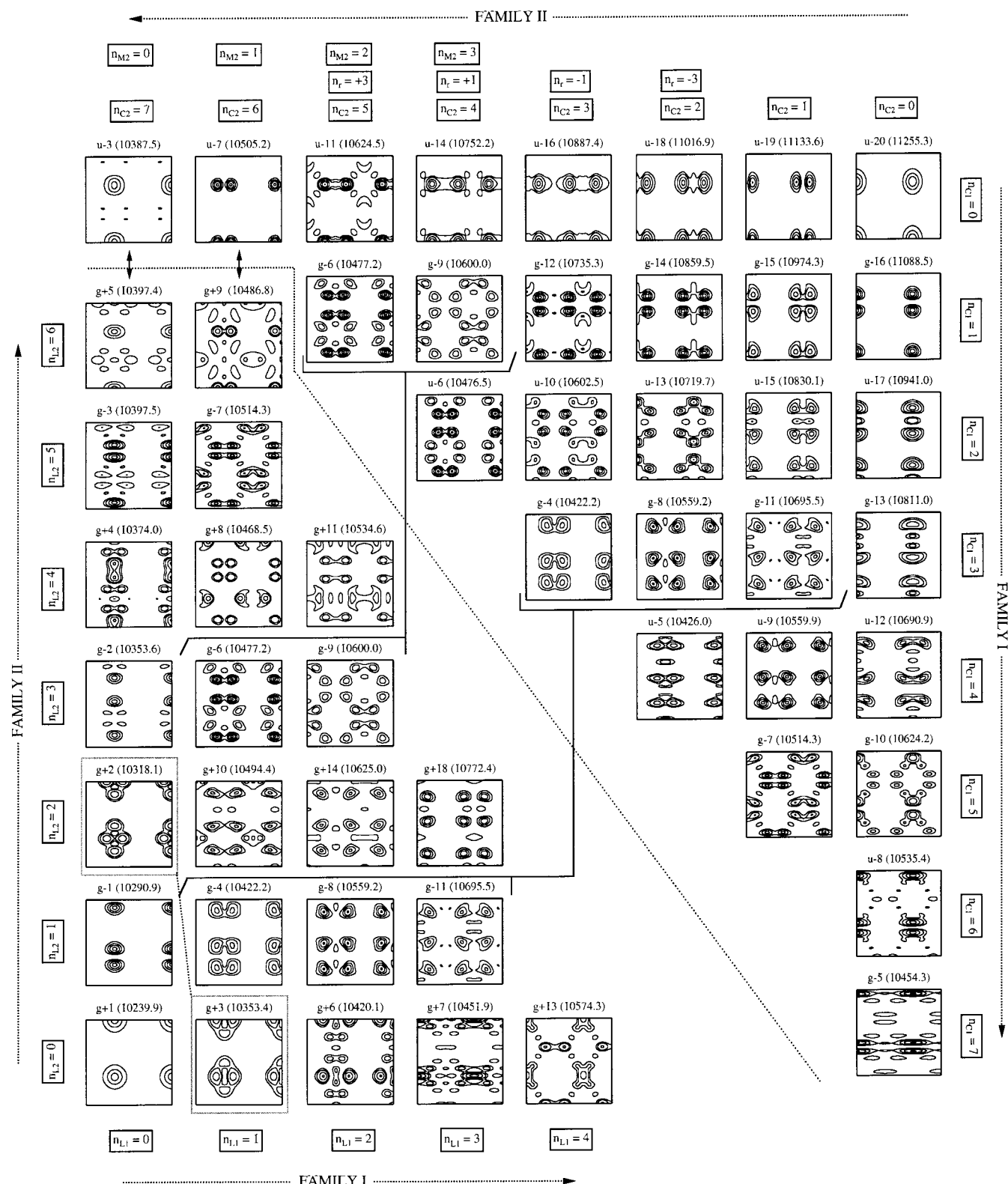
Figure 3. The arrangement of this figure is nearly identical to that of Figure 2, but with different symmetry classes. Specifically, the (n_{L1}, n_{L2}) assignments are provided for the $g+$ and $u+$ symmetry states, and the (n_{C1}, n_{C2}) assignments for the $g-$ and $u-$ symmetry states.

that when quantized yields its eigenenergy. The quantum numbers have dynamic meaning and are not just "indices" in a parametrized formula that gives the energy. The following sections demonstrate that this assignment can only be fully accomplished by utilizing simultaneously methods of nonlinear classical mechanics, quantum mechanics, and semiclassical mechanics.

Having provided an overview of the results, we now briefly

review the approach that makes the assignments possible, leaving details for the sections that follow. The first critical point is that no potential energy surface has been used. Rather, the dynamics of the system are represented by an algebraic spectroscopic effective Hamiltonian that has been fitted to experimental data with up to 15 000 cm^{-1} of vibrational excitation.[11] In fact, no PES exists with sufficient accuracy, but even if one did exist, the effective Hamiltonian approach (which

trivially yields an action/angle classical Hamiltonian) possesses a critical advantage over performing variational quantum and/or classical periodic orbit analysis on a potential energy surface. Specifically, in an action/angle Hamiltonian, every constant of the motion can be used in a canonical transformation to reduce the dimension of the problem.[5,7,12,13,17] Reduced dimensionality is helpful not only for computational expediency but also can be critical to a successful semiclassical analysis. Generically it is difficult to visualize the wave functions and to visualize and calculate the periodic orbit structures in more than two dimensions. This is not to say that by using certain well-chosen orthogonal coordinates, e.g., normal or local modes, that some wave functions will not reveal nodal patterns that infer the dynamics.[11] However, a complete coordinate-independent analysis cannot be done in this way; in the context of this work, we found that only states at the top and bottom of the polyads yielded to such a visual analysis.

We also wish to mention briefly a somewhat more subtle advantage of the action/angle approach in this particular study. As mentioned briefly above, the two families of periodic orbits merge at the top and bottom of the polyad. This is not a coincidence. The classical phase space contracts to a point at both energy extremes, and two periodic orbits must emerge (in the sense of a periodic orbit bifurcation diagram) out of each point (which give rise to the two families of periodic orbits). The classical dynamics is thus guaranteed to be simple at both the top and bottom, and although the periodic orbits evolve in more complicated ways in the middle of the polyad, the phase space structure never becomes too complicated. We found the ability to follow the periodic orbits from both the top and bottom of the polyad to be a great advantage in this study. In contrast, when using a potential energy surface, the classical phase space contracts to a point only at zero energy, and there are no constrictions at higher energies, making the identification of periodic orbits more difficult.[19]

The weakest point of our analysis is that the transformation between the action-angle variables and the physical space coordinates is in principle not known. [This would not be the case if the effective Hamiltonian had been derived by high-order perturbation theory (Van Vleck[7] or Gustavson[17] or as in refs 20−22) from a suitable potential energy surface; the perturbation theory approach solves for the action/angle variables of the system in terms of the original physical coordinates of the molecule and hence effectively solve the Hamilton-Jacoby equations for the system.[23]] As such, the periodic orbits in the action/angle space can be represented only approximately as physical motions of the molecule; here we have done so by employing a low order normal mode expansion for the action-angle and physical space variables. The justification for this approximation is as follows: First, there are examples where the perturbation theory expressions for the actions and angles were worked out to high order and the approximation was seen to be quite accurate,[6,7,17] certainly accurate enough for the pictorial description of the motions given here. Additionally, the results from effective Hamiltonian models compare well to eigenvectors of $H = T + V$ computed on usual (e.g., DVR) basis sets.[24−27] On a deeper level the resulting high order perturbation theory expressions for the spectral Hamiltonian (that look like eqs 7−10 below) are complex functions of *the original* simple action and angle variables. As such the Hamiltonian, the resulting trajectories and the expressions for the effective frequencies carry the burden of complexity that allows the final action and angle variables to remain simple and near the original ones. Similar things are seen in higher order perturbation theory

where matrix elements of complicated operators are computed in a basis of simple unperturbed states.

3. Hamiltonian and Methodology

The model of the acetylene bend degrees of freedom that is studied in this paper is an effective Hamiltonian that has been demonstrated to reproduce all observed "pure bending" vibrational levels of acetylene up to 15 000 cm^{-1} to a root-mean-square accuracy of better than 1.5 cm^{-1}.[10] This Hamiltonian model has resulted from years of work on acetylene by a number of researchers, notably by Plíva,[1] Herman and co-workers,[8] and Field and co-workers.[10] Both the quantum Hamiltonian and the procedure for converting it to a classical (action/angle) Hamiltonian have been detailed previously,[5,10,11,13,17,18] so we provide only a brief review here. The quantum effective Hamiltonian is defined in terms of the shift operators for the two-dimensional harmonic oscillator, and contains 16 empirically fitted parameters:

$$\hat{H}_Q = \hat{H}_Q^{lin} + \hat{H}_Q^{anh} + \hat{H}_Q^{int} \tag{1}$$

where

$$\hat{H}_Q^{lin} = \omega_4 \hat{v}_4 + \omega_5 \hat{v}_5 \tag{2}$$

$$\begin{aligned}
\hat{H}_Q^{anh} = {} & x_{44}\hat{v}_4\hat{v}_4 + x_{45}\hat{v}_4\hat{v}_5 + x_{55}\hat{v}_5\hat{v}_5 + y_{444}\hat{v}_4\hat{v}_4\hat{v}_4 + \\
& y_{445}\hat{v}_4\hat{v}_4\hat{v}_5 + y_{455}\hat{v}_4\hat{v}_5\hat{v}_5 + y_{555}\hat{v}_5\hat{v}_5\hat{v}_5 + g_{44}\hat{l}_4\hat{l}_4 + \\
& g_{45}\hat{l}_4\hat{l}_5 + g_{55}\hat{l}_5\hat{l}_5 \tag{3}
\end{aligned}$$

$$\begin{aligned}
\hat{H}_Q^{int} = {} & s_{45}(\hat{a}_{4d}^\dagger \hat{a}_{4g}^\dagger \hat{a}_{5d}\hat{a}_{5d} + \hat{a}_{4d}\hat{a}_{4g}\hat{a}_{5d}^\dagger\hat{a}_{5g}^\dagger) + \\
& [r_{45}^\circ + r_{445}(\hat{v}_4 - 1) + r_{545}(\hat{v}_5 - 1)](\hat{a}_{4d}\hat{a}_{4g}^\dagger \hat{a}_{5d}^\dagger\hat{a}_{5g} + \\
& \hat{a}_{4d}^\dagger\hat{a}_{4g}\hat{a}_{5d}\hat{a}_{5g}^\dagger) + \frac{1}{4}[r_{45}^\circ + r_{445}(\hat{v}_4 - 1) + \\
& r_{545}(\hat{v}_5 - 1) + 2g_{45}] \cdot (\hat{a}_{4d}^\dagger \hat{a}_{4d}^\dagger\hat{a}_{5d}\hat{a}_{5d} + \hat{a}_{4g}^\dagger \hat{a}_{4g}^\dagger\hat{a}_{5g}\hat{a}_{5g} + \\
& \hat{a}_{4d}\hat{a}_{4d}\hat{a}_{5d}^\dagger\hat{a}_{5d}^\dagger + \hat{a}_{4g}\hat{a}_{4g}\hat{a}_{5g}^\dagger a_{5g}^\dagger) \tag{4}
\end{aligned}$$

The values of the various parameters in this model are listed in Table 2 of ref 10.

Note that we have divided the effective Hamiltonian into three parts. The superscript "lin" refers to the harmonic (linear) diagonal terms and "anh" to the anharmonic (nonlinear) contributions to the zero-order energies. The resonant interaction terms, which generate the off-diagonal matrix elements, are contained in the "int" term. This term in particular looks very complicated, but in fact it simply encodes harmonic oscillator scaling relationships for three important mechanisms for exchanging energy and vibrational angular momentum between the cis and trans bend modes; these resonances are called Darling Dennison I/II and vibrational *l*-resonance. A critical point about this effective Hamiltonian is that its matrix representation is block diagonal in the zero-order normal mode number representation, and each block of the matrix can be uniquely labeled by a pair of conserved *polyad* quantum numbers $N_b = v_4 + v_5$ (the total number of quanta of bend excitation) and $l = l_4 + l_5$ (the total vibrational angular momentum), which we here restrict to $l = 0$. These polyad numbers correspond to constants of motion in the classical Hamiltonian.

The classical Hamiltonian is derived from the quantum Hamiltonian in a two step process:

1. The quantum effective Hamiltonian, expressed in terms of shift operators, is converted to a classical action/angle Hamiltonian, using standard correspondence rules. [For those

who are unfamiliar with action/angle Hamiltonians, a few brief comments. Classical Hamiltonians are often written in terms of kinetic and potential energy with positions and momenta as the variables, but using actions and angles provides more transparent quantum-classical correspondence. The quantum analogue of an action is a quantum number; the classical angles, as will be seen below, contain information about resonances.] Specifically, the transformation is generated by the Heisenberg correspondence relations

$$\hat{a}_j \rightarrow \sqrt{I_j}\exp(-i\phi_j) \tag{5}$$

$$\hat{a}_j^\dagger \rightarrow \sqrt{I_j}\exp(+i\phi_j) \tag{6}$$

2. A canonical transformation is performed to transform the classical Hamiltonian from the initial action/angle coordinates $(4d, 5d, 4g, 5g)$ to a new set of action/angle coordinates. The new actions we label by J_a, J_b, K_a, and K_b, and the conjugate [corresponding] angles we call ψ_a, ψ_b, θ_a, and θ_b. The new actions are chosen such that K_a and K_b correspond (up to a multiplicative factor, and neglecting zero-point corrections) to the quantum polyad numbers N_b and l; that is, K_a and K_b are constants of the motion (they do not change during any classical trajectory), and we can consider the classical Hamiltonian to depend *parametrically* on these conserved actions. Thus, by exploiting the existence of the two conserved quantities, we reduce a 4 degree of freedom problem to a 2 degree of freedom problem, which is described by the actions (J_a, J_b) and angles (ψ_a, ψ_b).

The final classical Hamiltonian takes the form:

$$H_C = H_C^{lin} + H_C^{anh} + H_C^{int} - E^\circ \tag{7}$$

$$H_C^{lin} = 2\omega_4(K_a + J_a) + 2\omega_5(K_a - J_a) \tag{8}$$

$$
\begin{aligned}
H_C^{anh} = {} & 4x_{44}(K_a + J_a)^2 + 4x_{45}(K_a + J_a)(K_a - J_a) + \\
& 4x_{55}(K_a - J_a)^2 + 8y_{444}(K_a + J_a)^3 + \\
& 8y_{445}(K_a + J_a)^2(K_a - J_a) + 8y_{455}(K_a + J_a)(K_a - J_a)^2 + \\
& 8y_{555}(K_a - J_a)^3 + 4g_{44}(K_b - J_b)^2 + \\
& 4g_{45}(K_b - J_b)(K_b + J_b) + 4g_{55}(K_b + J_b)^2
\end{aligned} \tag{9}
$$

$$
\begin{aligned}
H_C^{int} = {} & 2s_{45}[(K_a^2 - K_b^2)^2 + (J_a^2 - J_b^2)^2 - \\
& 2(K_a^2 + K_b^2)(J_a^2 + J_b^2) - 8K_aK_bJ_aJ_b]^{1/2}\cos(\psi_a) + \\
& 2[r_{45}^\circ + r_{445}(2(K_a + J_a) - 1) + \\
& r_{545}(2(K_a - J_a) - 1)]\cdot[(K_a^2 - K_b^2)^2 + (J_a^2 - J_b^2)^2 - \\
& 2(K_a^2 + K_b^2)(J_a^2 + J_b^2) - 8K_aK_bJ_aJ_b]^{1/2}\cos(\psi_b) + \\
& {}^1\!/_2\{r_{45}^\circ + 2g_{45} + r_{445}[2(K_a + J_a) - 1] + \\
& r_{545}[2(K_a - J_a) - 1]\}\cdot\{[(K_a + K_b)^2 - \\
& (J_a - J_b)^2]\cos(\psi_a - \psi_b) + [(K_a - K_b)^2 - \\
& (J_a + J_b)^2]\cos(\psi_a + \psi_b)\} \tag{10}
\end{aligned}
$$

Here we have introduced E° to account for the quantum mechanical zero-point energy. Note that the diagonal harmonic and anharmonic terms from the quantum effective Hamiltonian are expressed solely in terms of the classical actions J_a, which corresponds to $v_4 - v_5$, and J_b, which corresponds to $l_4 - l_5$. The "interaction" terms, which are the classical analogues of
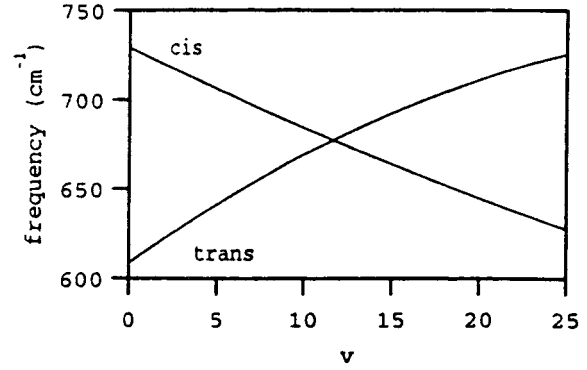

Figure 4. The classical frequencies of the zero-order normal mode motions, as a function of the number of quanta of excitation (classical action). The crossing of the frequencies at $N_b \approx 12$ results in a restructuring of the classical mechanics.

the quantum resonance terms (off-diagonal matrix elements), involve the classical angles in addition to the actions.

In the Introduction, we suggested that the $N_b = 16$ polyad was particularly interesting, and challenging, from the standpoint of semiclassical analysis due to the prominence of chaos, which in turn is due to the near degeneracy of the trans and cis bend frequencies. Having defined our Hamiltonian, we can now justify this assertion from a classical mechanical point of view. Specifically, in classical mechanics, the frequency of a particular type of motion can be obtained as

$$\omega(J) = \frac{\partial H}{\partial J} \tag{11}$$

where H is the classical Hamiltonian (the classical energy) and J represents some classical action. The quantum mechanical analogue of the action is a quantum number, and thus we can obtain nominal frequencies for the bend modes in the context of the effective Hamiltonian as

$$\omega(v_b) = \frac{\partial \hat{H}}{\partial v_b} \tag{12}$$

where b is 4 or 5. These quantities are plotted in Figure 4. Note how the frequencies cross at $N_b \approx 12$. When the classical frequencies become equal, the individual modes become maximally susceptible to perturbations (i.e., the coupling terms in H^{int}). In practice, the classical mechanics begins to change even before the normal-mode frequencies become equal, but past the point at which they cross, the classical mechanics undergoes a fundamental change. One of the symptoms of this transition is an explosion of classical chaos in the middle of the polyads, which is particularly prominent at $N_b = 16$ (the dynamics gradually becomes more regular at higher bend excitation).

4. Classical Dynamics

From this point onward we will be concerned exclusively with $N_b = 16$ and $l = 0$. In terms of classical mechanics, our primary task is to elucidate the periodic orbit structure, which, as has been suggested above, constitutes the critical framework for investigating quantum-classical correspondence.

An essential tool for identifying the periodic orbits are surfaces of section, which are slices through the classical phase space. Note that the exploitation of the polyad quantum numbers makes possible the use of surfaces of section. As explained above, the bending system of acetylene has 4 degrees of freedom

(two doubly degenerate bend modes), but the 2 conserved polyad quantum numbers reduce the effective dimensionality to 2 degrees of freedom, which corresponds to a four-dimensional phase space (a position and momentum for each degree of freedom, or in our case, an action and an angle). However, energy conservation effectively constrains the dynamics to three dimensions within the phase space. Thus, to reduce the dynamics to a 2D plot, we need only to specify the value of one of the coordinates. In practice, various surfaces of section (slices) can be taken along the different coordinates to be sure that one has a full view of the dynamics. The power of surfaces of section is that they immediately allow one to identify (1) the extent of chaos at a given energy (chaos looks like randomly scattered points on the surface) and (2) the stable periodic orbits, which are located in the middle of the sets of concentric circles, which result from trajectories that lie on "torus bundles": regular regions of phase space that surround the central periodic orbit fiber.

Quantum mechanically, the finite number of eigenstates of a polyad span a finite energy range. Similarly, once the conserved quantities K_a and K_b (classical polyad numbers) have been specified, only a finite range of classical energy is accessible. The accessible energy range for any given polyad can be obtained by a straightforward but tedious calculation, as described in ref 13. In the analysis below, we take advantage of the fact that, at the extreme high and low energies of the polyad, only a single point in the space of classical angles (ψ_a, ψ_b) is accessible; this can only occur once the classical frequencies of the trans and cis bend motions come into resonance. Having found these limiting energies, we focus on enumerating the important periodic orbits that exist within the polyad as a function of energy. We present a schematic "bifurcation diagram" in the center of Figure 1 which summarizes the periodic orbit structure. The word "bifurcation" refers to events in which new periodic orbits are born and/or where existing periodic orbits cease to exist. Bifurcations are thus of primary importance in the context of describing the overall classical structure, and by implication, to understanding the quantum structure from the standpoint of quantum-classical correspondence.

In addition to the surfaces of section in Figure 1, which are the "raw" classical data, and the bifurcation diagram, which summarizes the periodic orbit structure, we present two other types of plots in our overview of the classical dynamics. Each of these two types of plots represents the classical motions associated with the periodic orbits. The first projects this motion onto the (ψ_a, ψ_b) plane. The advantage of this representation is that it is two-dimensional, and as will be seen below, is optimal for establishing correspondence with the quantum mechanical eigenfunctions, which will be projected into the same space. The disadvantage of this representation is that it is highly abstract. That is, motions in the (ψ_a, ψ_b) space do not have any obvious interpretation in terms of the physical motions of the two hydrogens in acetylene.

However, as mentioned in section 2, it is possible to reconstruct the physical molecular motions from the abstract-space dynamics by a mathematical transformation that we call a "lift". This lift essentially corresponds to undoing the dimensionality reduction and the canonical transformation that defined the abstract a/b coordinates in terms of the more physically intuitive cis and trans bend (dimensionless) normal coordinates. We refer readers interested in a detailed derivation of the lift procedure to ref 13. It should be noted that the lift cannot specify the precise bond lengths or angles of the
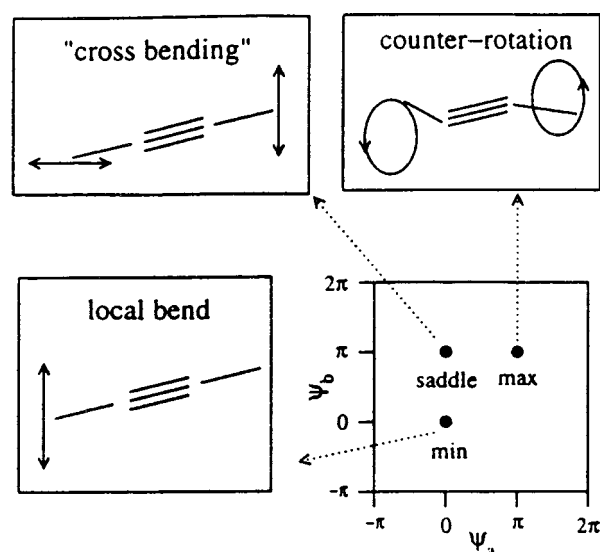

Figure 5. The physical molecular motions associated with the three fixed points in the abstract (ψ_a, ψ_b) space: (0, 0), which corresponds to the minimum energy within the polyad and lifts to a local bend motion; (0, π), the saddle point, which lifts to a motion in which the two hydrogens bend with identical amplitudes but in orthogonal planes; and (π, π), the maximum energy point, which lifts to the counter-rotational motion. The periodic orbits at other energies within the polyad vary smoothly between these three limiting types of motion.

molecule. This is not a deficiency of the mathematical transformation but rather a generic deficiency of fitted spectroscopic effective Hamiltonians, in which the coordinates are not explicitly defined. This is not a serious problem, however. Our concern is not, e.g., whether the hydrogens bend by 65° versus 70° in a particular type of motion, but rather with the qualitative aspects of the motion: How are the motions of the two hydrogens correlated? Do they bend through linearity (only possible if they have zero angular momentum) or do they undergo circular motions? Does one hydrogen undergo much larger amplitude motion than the other? From a practical standpoint, we plot the "lifted" motions as dimensionless (x, y) displacements of the two hydrogens from the CC axis.

Repeated reference to Figures 1 and 5 will be useful from here on. In fact, for the reader interested in just the flavor of what is done and pictures of the resulting motions, a study of these figures may serve as substitute for a detailed reading of the rest of this section.

Before proceeding further, we examine the "lift" associated with three special points in the (ψ_a, ψ_b) plane: (0, 0), (π, π), and (0, π). As mentioned above, at the energy extremes of the polyad, the classical phase space contracts to single points in the (ψ_a, ψ_b) plane. Specifically, at the low energy extreme of the polyad, the phase spaces contracts around (0, 0), while the point (π, π) plays the analogous role at the top of the polyad. The point (0, π), on the other hand, which becomes accessible at $E = 10\ 322$ cm^{-1} (in the middle of the polyad), can be considered a saddle point of the dynamics, because the second derivative of the energy with respect to ψ_a is negative while that with respect to ψ_b is positive at this point.

The significance of each of these three points will be considered in some detail below. For now, we simply state that each of these points "lifts" to a particularly simple molecular motion, and these three motions play special roles in the semiclassical assignments. As can be seen in Figure 5, the point (0, 0) lifts to a local bend motion. That is, at the lowest possible energy within the polyad, the only classical motion that is possible is a perfect local bend, in which one hydrogen bends

while the other is perfectly stationary. At the top of the polyad, the point (π, π) lifts to a counter-rotation motion, in which the hydrogens undergo perfect circular motions, and the molecule never passes through linearity (note that the two hydrogens must rotate in opposite directions to maintain zero vibrational angular momentum). Finally, the saddle point $(0, \pi)$ lifts to a motion in which the two hydrogens vibrate with identical amplitudes but in orthogonal planes.

The contraction of the accessible (ψ_a, ψ_b) configuration space at the top and bottom of the polyad implies that the classical mechanics will be particularly simple near these points, and thus we begin our overview of the dynamics in the $N_b = 16$ polyad at its two energy extremes, before working inward toward the complicated middle of the polyad. In the immediate vicinity of the extremal points in the polyad, the energy is nearly quadratically dependent on the classical angles. In analogy with a 2D oscillator, there are two stable motions that emerge from both the top and bottom of the polyad, and these run along the ψ_a and ψ_b coordinates (oscillating about $(0, 0)$ at the bottom of the polyad and about (π, π) at the top). That is, the pairs of periodic orbits that emerge from the extremal points are in some way analogous to the normal modes of a 2D oscillator. As we have already emphasized, the dynamics in the *a/b* space is quite abstract, but the lift procedure can again give us insight into the physical motions of the molecule associated with the periodic orbits near but not at $E_{\min}$ or $E_{\max}$.

Consider first the two periodic orbits that emerge from the point $(\psi_a = 0, \psi_b = 0)$ at the bottom of the polyad, which we label L_1 and L_2. The label "L" stands for "local bend", since it can be anticipated that L_1 and L_2 must both be closely related to the local bending associated with the extremal point $(0, 0)$. The L_1 periodic orbit, which runs along ψ_a, differs from a pure local bend in that the second hydrogen, which in the perfect local bend does not move at all, gains a small amount of vibrational excitation, in the same plane as the first hydrogen. The L_2 periodic orbit, which runs along ψ_b, also involves a small amount of excitation in the second hydrogen, but this time in an orthogonal direction to the motion of hydrogen 1. Thus, the L_1 and L_2 periodic orbits each describe an "imperfect" local bending motion [in a technical sense, they can be referred to as normal modes of the deviation from pure local bending behavior]. As energy increases above $E_{\min}$, and the periodic orbits sample regions of the (ψ_a, ψ_b) configuration space that are further from $(0, 0)$, the corresponding lifted motions become increasingly imperfect; the fate of these motions will be considered below.

Similarly, at the top of the polyad, the C_1 and C_2 periodic orbits represent imperfect counter-rotation motions. The perfect counter-rotation involves the hydrogens tracing out perfect circles in planes perpendicular to the CC axis. Both the C_1 and C_2 periodic orbits involve an elongation of the motion into an ellipse which precesses with time.

We now turn to the more complicated dynamics in the interior of the polyad, and in particular examine how the periodic orbits at the top and bottom of the polyads are linked to each other. When examining the surfaces of section, the "raw data", it is not immediately obvious that the low and high energy periodic orbits link to each other in any simple way. A number of bifurcations occur in the intermediate energy regime, and at most energies chaos dominates. However, within the chaos there exist slightly unstable periodic orbits that can be followed numerically, and it is found that L_1 connects with C_1 and L_2 links with C_2 (mediated by other periodic orbits that are born out of bifurcations). Moreover, although the periodic orbits in 2D

change their topology radically (e.g., from librators to rotators) as energy increases in the polyad, the dynamical evolution of the modes in the full, physical space is gradual and seemingly continuous on the scale of quanta of energy.

Many of the qualitative changes in the classical mechanics in the middle of the polyad can be understood in terms of the topology of the abstract (ψ_a, ψ_b) configuration space as a function of energy. Near the extreme high and low energy points, the dynamics is constrained to remain near (π, π) and $(0, 0)$, respectively. In the middle of the polyad, however, all values of ψ_a and ψ_b become accessible, leading to much more complicated dynamics. Starting from the bottom of the polyad and working upward in energy, the accessibility of the configuration space opens up in two steps. First, at $E = 10\ 322\ cm^{-1}$, all values of ψ_b become accessible. Second, at $E = 10\ 434\ cm^{-1}$, all values of ψ_a become accessible (and thus all of configuration space is accessible).

The saddle point at $(\psi_a = 0, \psi_b = \pi)$, which becomes accessible at $E = 10\ 322\ cm^{-1}$, is the most important organizing center for the dynamics in the middle of the polyad. On a real 2D potential energy surface, a saddle point would be associated with two "normal modes", one with an imaginary frequency which runs along the direction with the negative second derivative, and one with a real frequency along the orthogonal coordinate with the positive second derivative. The situation here is analogous. The L_2 periodic orbit, which runs along ψ_b, begins to rotate along ψ_b at $E = 10\ 322\ cm^{-1}$ (this would be analogous to the mode with the imaginary frequency). Simultaneously, a new periodic orbit, M_2, is born at the saddle point which, at least initially, undergoes bounded motion in the ψ_a direction (this corresponds to the mode with the real, positive frequency). [In a technical sense, we say that L_2 is homoclinic to M_2 when it is born. Also, it should be noted that L_2 becomes unstable at $10\ 281\ cm^{-1}$ and in rapid succession a number of very similar and mostly unstable periodic orbits are born; we refer to these collectively as L_2, and those that rotate as L_2^r.]

As M_2 begins to sample regions of configuration space further from the saddle point, the physical motion of the hydrogens increasingly acquires rotational character. This is significant because it anticipates the connection of M_2 with C_2, which is primarily "counter-rotational" in character. The connection between these orbits is actually quite simple in the abstract *a/b* space. At $10\ 434\ cm^{-1}$, all values of ψ_a become accessible, and slightly above this energy $(10\ 503\ cm^{-1})$ the M_2 motion is no longer trapped near $(0, \pi)$ but instead starts rotating along ψ_a (we rename it M_2^r to reflect this fact). This rotating motion persists until $11\ 183\ cm^{-1}$, which is the highest energy at which all of configuration space is accessible. In contrast to the case at the bottom of the polyad, where rotational motion in the ψ_b direction became possible before rotational motion in the ψ_a direction, at the top of the polyad both directions become accessible (or inaccessible, for decreasing energy) at once, which occurs at $E = 11\ 183\ cm^{-1}$. At this energy, the rotating M_2^r periodic orbit connects with the librating [about (π, π)] C_2 orbit.

In the above discussion of the Family 2 orbits, we omitted many details of the classical dynamics, such as the stabilities of the periodic orbits. The M_2^r periodic orbit, for example, is initially unstable; as can be inferred from the surfaces of section, classical chaos dominates at $E \approx 10\ 500\ cm^{-1}$. However, M_2^r becomes stable at higher energies $(E > 10\ 690\ cm^{-1})$, and in fact organizes the only sizable stable region within the classical chaos (EBK quantization will be applied to this torus in the next section). For a more detailed discussion of the classical dynamics, the reader is referred to ref 13; this paper treats the

$N_b = 22$ polyad and not $N_b = 16$, but key qualitative aspects of the classical dynamics are similar.

The connection between L_1 and C_1 proceeds along similar lines as the connection between L_2 and C_2, but one major difference is that the point ($\psi_a = \pi$, $\psi_b = 0$), unlike $(0, \pi)$, is not a saddle point. Thus, M_1^r, which indirectly connects L_1 to C_1, is not born in the same manner as M_2, which was associated with the saddle point. The L_1 periodic orbit rotates for $E > 10\,490$ cm^{-1} and C_1 can rotate for $E < 11\,015$ cm^{-1}. The M_1^r periodic orbit, however, does not directly connect the L_1 and C_1 orbits, which run in orthogonal directions. Rather it connects L_{1a} with C_{1a}, which are born out of bifurcations with the original L_1 and C_1 orbits, and which are more complicated motions that run roughly, but not exactly, along ψ_a and ψ_b respectively. The M_1^r motion itself is very complicated, although it can clearly be considered a compromise between the L and C motions, in the sense that the hydrogens tend to oscillate along one of two orthogonal directions, but with superimposed rotational motion (and periodic switching of the dominant axis).

5. Semiclassical Eigenstate Assignments

At the end of this section we perform EBK quantization on certain of the stable tori in the classical mechanics to establish rigorous, numerical quantum-classical correspondence. This will not assign the majority of states but will act as a check on our prime method of assignment which is node counting along periodic orbits. Carrying out the node counting is not always a visually obvious procedure. We now outline what we actually do. We first establish quantum-classical correspondence qualitatively between wave functions and periodic orbits (which are motions) by plotting wave functions and isoenergetic (accounting for zero-point energy) periodic orbits in the same set of coordinates. Various sets of coordinates in principle could be chosen. The quantum effective Hamiltonian is defined in terms of shift operators for the 2D harmonic oscillator, which may be represented in either rectilinear (x, y) or radial (ρ, ϕ) coordinates. The radial coordinates are somewhat more convenient, because conservation of angular momentum implies that only three coordinates, $(\rho_4, \rho_5, \phi = \phi_4 - \phi_5)$, are needed to represent the wave functions. Such coordinates were used in an earlier, quantum mechanical study of the acetylene bend modes.[11] An example of quantum-classical correspondence in these coordinates is provided in Figure 6 of ref 14, but in general it is inconvenient to attempt to compare orbits and eigenfunctions in a three-dimensional space.

A better choice of coordinates is the two-dimensional abstract space of (ψ_a, ψ_b). The periodic orbits have already been represented in this space, and it is straightforward to represent the quantum eigenfunctions in this space as well, by introducing a semiclassical basis set defined by

$$\Phi = \exp(ij_a\psi_a)\exp(ij_b\psi_b) \qquad (13)$$

where j_a and j_b are semiclassical quantum numbers; the canonical transformation that we have utilized to convert from the original normal mode coordinates to the abstract a/b space implies that

$$j_a = \frac{v_4 - v_5}{4} \qquad (14)$$

$$j_b = \frac{l_4 - l_5}{4} \qquad (15)$$

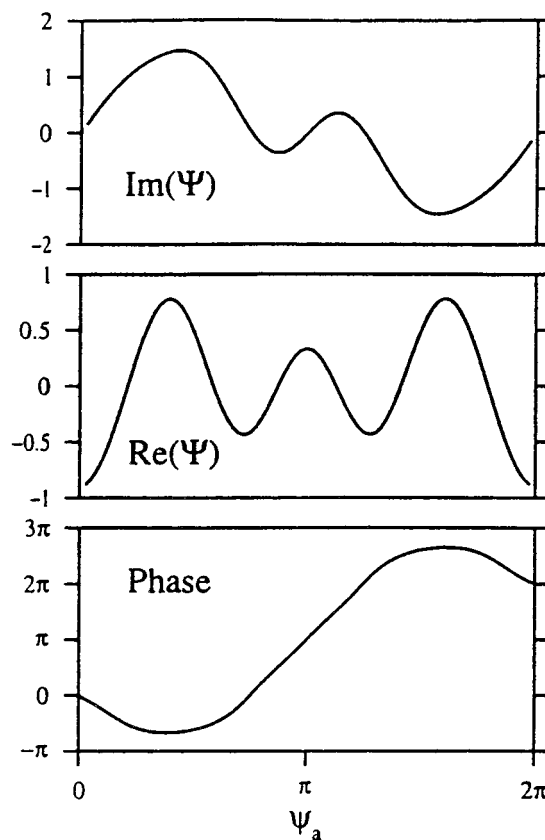The wave functions should really be viewed as being wrapped

Figure 6. The real and imaginary parts of the wave function E_{16}^{g+} along ψ_a with $\psi_b = \pi$, as well as the phase advance, which provides the assignment n_r (along the rotating periodic orbit M_2^r).

onto a two-dimensional torus defined by the classical angles (ψ_a, ψ_b). That is, the wave functions are periodic in both coordinates from 0 to 2π, but in Figures 2 and 3, we choose to show a larger range on both axes so as not to cut the wave functions at inconvenient points. This is particularly important because, as will be seen below, the eigenfunctions tend to have their probability localized near one of the three fixed points of the classical mechanics, $(0, 0)$, $(0, \pi)$, and (π, π). For further details of our semiclassical eigenfunctions, please refer to section V of ref 13.

The semiclassical eigenfunctions for all of the states in the $N_b = 16$ polyad are represented in Figures 2 and 3 (some of the states are actually represented twice; the layout of these figures will become clear below). The eigenstates are arranged according to their symmetries and their semiclassical assignments. Below, we use the notation $E_n^{g/u \; +/-}$ to label the eigenstates. The superscript indicates the symmetry of the state and the subscript indicates the energy rank of the state among all other states within the polyad of the same symmetry. There are four symmetry classes of states, which are described by the g/u symmetry (with respect to the center of inversion of the molecule) and $+/-$ parity.

Our strategy for making the eigenstate assignments once again involves working inward from the energy extremes of the polyad. Given that the classical dynamics near the energy extremes is largely regular, confined to a relatively small region of phase space, and dominated by a handful of periodic orbits, it is unsurprising that the semiclassical assignments, which can be checked by using the EBK method, are straightforward in these energy regimes. The lowest and highest energy eigenstates in the polyad are of course localized around $(0, 0)$ and (π, π), respectively; somewhat less obvious is that the high- and low-

lying eigenstates can be grouped into symmetry pairs. The pairs of eigenstates E_1^{g+} (Figure 2) and E_1^{u+} (Figure 3), for example, both look simply like two-dimensional Gaussians centered around (0, 0), and their eigenenergies differ by only 4×10^{-6} cm^{-1}. Many of the other low-lying eigenstates within the polyad can also be organized into symmetry pairs with the same parity but opposite g/u symmetry. The eigenstates with the highest energies within the polyad, on the other hand, occur for pairs with *both* opposite parity *and* opposite g/u symmetry.

This symmetry pairing has been explained previously. In ref 11, simple symmetry arguments are used to predict that local bend states should appear in $g+/u+$ and $g-/u-$ pairs, while counter-rotational states should occur in $g+/u-$ and $g-/u+$ pairs. The argument with respect to the local bend states is fairly simple. Classically, the local bend motion corresponds to a single hydrogen bending, but the indistinguishability of the hydrogens in quantum mechanics implies that the eigenstates must be symmetric (g) or antisymmetric (u) combinations of the two equivalent local bends. The argument with respect to counter-rotation is somewhat more complicated and relies on the indistinguishability of the two senses of rotation (clockwise vs counterclockwise). These symmetry arguments were extended and generalized in ref 13, where it was shown that any eigenfunctions with probability density localized primarily near $\psi_b = 0$ will appear in g/u pairs, while those localized near $\psi_b = \pi$ appear in pairs with opposite parity and g/u symmetry. This more general argument implies that states localized near the saddle point $(0, \pi)$ (see below) will also appear in symmetry pairs.

In addition to the very lowest energy eigenstates, E_1^{g+} and E_1^{u+}, a handful of other low-lying eigenstates can be assigned trivially by inspection of their nodal patterns. For example, E_1^{g-} and E_1^{u-} can be assigned as ($n_{L1} = 1$, $n_{L2} = 0$); that is, they have one node along the L_1 periodic orbit, which runs along the ψ_b direction, and no nodes in the orthogonal coordinate. The symmetry pairs E_2^{g+}/E_2^{u+} and E_3^{g+}/E_3^{u+} do not have such an obvious assignment. This can be explained in terms of an accidental near-degeneracy of the semiclassical states ($n_{L1} = 0$, $n_{L2} = 2$) and ($n_{L1} = 1$, $n_{L2} = 0$), which mix to yield the more complicated eigenstates [that is, adding and subtracting the mutually perturbed pairs of states yields states with nearly perfect semiclassical assignments]. These types of mixings are also observed at higher energies, in the middle of the polyad (E_{12}^{g+} and E_{13}^{g+} are another easily identifiable mutually perturbing pair).

The assignments of other states at low energy, even when such mixings do not play a role, are not always immediately obvious on a first viewing, but can be firmly established upon careful inspection, particularly by the use of *slices through the eigenfunctions along the periodic orbits*. As an example, consider the symmetry pair E_8^{g-}/E_9^{u-}, which is assigned as ($n_{L1} = 2$, $n_{L2} = 1$). It is not immediately obvious that there are 2 nodes along the L_1 periodic orbit, which runs along the ψ_a direction, primarily due to the small amplitude of the middle lobes and their distortion from a straight line. Slices through the wave function however make the assignment clear. The distortions of the wave function are not due to accidental mixings in this case. Rather, these distortions reflect the underlying classical mechanics. The L_1 orbit becomes unstable just slightly above E_{min} and undergoes a series of bifurcations, the most important of which gives birth to the L_{1a} orbit. The quantum eigenstates reflect some averaged contribution from the various closely related Family 1 periodic orbits that exist at this energy. This type of effect is more extreme in, e.g., E_{14}^{g+},

which clearly reflects the L_{1a} periodic orbit, which bends away from the $\psi_b = 0$ axis; that is, most of the probability density in this state is localized near the turning points of the L_{1a} orbit.

Once the effects of semiclassical state "mixing" and other distortions of the eigenfunctions are taken into account, all of the eigenstates within the $N_b = 16$ polyad can be organized according to the number of quanta of excitation along the two families of periodic orbits. The symmetry pairings aid in the assignment process, although the energy splittings are larger in the middle than at the energy extremes of the polyad. In addition, as will be discussed below, several of the eigenstates have also been rigorously assigned using EBK quantization. Our confidence in the assignments, however, ultimately rests on the regularity that can be observed in the progressions of eigenstates in Figures 2 and 3.

Several of the eigenstates are multiply assigned, such as E_{11}^{g-}. This eigenstate shows little probability density in the immediate vicinity of either (0, 0) or (π, π), and can be assigned nearly equally well as either ($n_{L1} = 3$, $n_{L2} = 1$) or ($n_{C1} = 3$, $n_{C2} = 1$). This double assignment should not be seen as a deficiency of the semiclassical approach. Rather, the ability to provide two assignments for several eigenstates simply reflects the fact that the L and C periodic orbits connect with each other in a smooth manner. A state such as E_{16}^{u+} clearly can be assigned as ($n_{C1} = 1$, $n_{C2} = 3$) but is also doubly assigned as ($n_{L1} = 3$, $n_{L2} = 2$), because it can be considered to continue the series of states with $n_{L2} = 2$.

The role of the saddle point, and that of the M_2/M_2^r periodic orbits, in connecting between the L and C assignments deserves careful consideration. Starting from low energy, the series of states with $n_{L1} = 0$ and increasing n_{L2} gradually begin to probe the vicinity of the saddle point. At energies above that of the saddle point, the L_2 periodic orbit can begin to rotate along the ψ_b direction, but the classical motion proceeds most slowly at the saddle point, causing the quantum probability density to accumulate there. The state E_3^{u-} provides a very clear example of this effect. This state can be assigned as ($n_{L1} = 0$, $n_{L2} = 5$), because five nodes can be counted along ψ_b between $-\pi$ and π. However, this state can also clearly be assigned as the "zero-point level" associated with the saddle point, since it is very strongly localized around $(0, \pi)$. This particular state, and its symmetry partner E_5^{g+}, demarcate the transition between state assignments using the (n_{L1}, n_{L2}) and the (n_{C1}, n_{C2}) labels. In the immediate vicinity of the saddle point energy, however, assignments in terms of the n_{M2} periodic orbit, which is born at the saddle point, are appropriate. The state E_7^{u-}, for example, can be labeled with $n_{M2} = 1$, although it should be noted that it can also be formally labeled as $n_{C2} = 6$, by following the series of counter-rotation states downward in energy (the latter assignment provides less physical insight).

Thus, the assignments in terms of M_2 and C_2 can be connected with each other, and through the saddle point, they can be connected with the assignments in terms of L_2. We have not explicitly considered at this point assignments in terms of the M_2^r periodic orbit. This is simply the rotating orbit that links M_2 with C_2, and in some sense providing assignments in terms of M_2^r would seem superfluous. However, the rotating character of this orbit changes the nature of the assignments. At this point, a more careful discussion of the semiclassical basis set is in order.

First, note that the zero-order normal mode states, which constitute the basis set of the effective Hamiltonian, all have a completely "flat" probability distribution in the (ψ_a, ψ_b) plane (using the definition of the semiclassical basis in eq 13). That

is, there is an equal probability of finding the system at any chosen value of ψ_a and ψ_b. The normal mode states can only be distinguished by inspecting the real and imaginary portions of the wave functions. The eigenstates of the Hamiltonian, however, have probability localized in various portions of the (ψ_a, ψ_b) space due to the anharmonic resonant interactions that mix the zero-order, normal mode states. For example, the Darling-Dennison I resonance, which is parametrized by s_{45} and exchanges 2 quanta of trans and cis bend excitation, creates localization along the ψ_a coordinate (in the classical Hamiltonian, it is the term that involves cos ψ_a). The vibrational l-resonance, which exchanges vibrational angular momentum between the normal modes, creates localization along ψ_b. [The Darling-Dennison II resonance creates localization along both coordinates, but is numerically less important than the other two resonances.]

The net effect of these resonances is to localize the low-lying eigenstates near (0, 0) and the high-lying eigenstates near (π, π); that is, the resonances are responsible for lowering the energy of the point (0, 0) and raising that of (π, π), such that these points represent the energy extremes of the polyad. In the middle of the polyad, all of the angle space is accessible, and the eigenstates need not localize near any of the stationary points. Many of the states do continue to localize around one of the stationary points, but a notable exception are states such as E_{19}^{g+} and E_{14}^{u-}, which have probability localized almost exactly mid-way between the saddle point (0, π) and (π, π).

Although these states can be (doubly) assigned in terms of the number of quanta of excitation along M_2 [around (0, π)] and C_2 [around (π, π)], a more physically meaningful assignment can be obtained in terms of the number of quanta along M_2^r. These assignments we list as n_r. M_2^r is a rotating orbit, which by definition exists only when all values of ψ_a are accessible, and probability density accumulates along the orbit preferentially at those points where the motion is slowest, which is somewhere between 0 and π, depending on the precise energy. However, the localization of the probability density in these states is rather weak along the ψ_a direction; that is, although these states are highly localized along ψ_b, they are nearly plane waves along ψ_a. In a qualitative sense, this implies that the vibrational l-resonance plays a strong role in "shaping" these wave functions but that the Darling-Dennison resonances do not (that is, these eigenstates can be assigned the normal mode quantum numbers v_4 and v_5, but not l_4 or l_5). From the standpoint of semiclassical assignment, this fact implies that the states are best assigned by examining the real and imaginary parts of the wave function along ψ_a. Specifically, the assignment is provided by the phase advance α of the wave function, defined by

$$\tan \alpha = \frac{\text{Re}(\Psi)}{\text{Im}(\Psi)} \quad (16)$$

where Ψ is the complex valued wave function. We choose to define $n_r = \Delta\alpha/\pi$, where $\Delta\alpha$ is the change in phase from $\psi_a = 0$ to $\psi_a = 2\pi$. The quantum numbers obtained from this scheme can be either positive or negative. An example of the phase advance assignment is given in Figure 6, for the eigenstate E_{16}^{g+}, which is assigned as $n_r = +2$.

To verify these assignments we have successfully quantized by the EBK method the tori associated with M_2^r and found that the loop integrals $S = \oint J_a \text{d}\psi_a/2\pi$ take the values n_r for the states in question. The EBK quantization method can also be applied at higher energies and at slightly lower energies; at the bottom of the polyad, however, the regular structures in phase

space decay too rapidly to chaos for the EBK method to be feasible. At the top of the polyad, at the energy of the symmetry doublet E_{25}^{g+}/E_{20}^{u-}, there is one and only one torus structure, for which both loop integrals are very nearly equal to $^1/_2$ (i.e., only "zero-point" excitation). EBK quantization can also be carried out to confirm our assignments for several other states near the top of the polyad. At other energies, there are no torus structures of appreciable size, particularly between the energies of $\sim$ 10 300$-$10 700 cm^{-1}, and the EBK quantization method cannot be applied. However, with unstable periodic orbits, one can still carry out the loop integral in one dimension (along the unstable orbit), even though it is not possible to carry out the integral in the transverse direction, as in the EBK method. For example, we have carried out the loop integrals along the unstable M_2 periodic orbit near the saddle point energy. The doublet pair E_5^{g+}/E_3^{u-}, which represents the zero-point level associated with the saddle point, lies at an energy which is very close to the energy where M_2 has action $^1/_2$. Similarly the doublet pair E_9^{g+}/E_7^{u-} occurs at an energy where the action of M_2 has the value $^3/_2$.

6. Conclusion

The pure bending eigenstates of acetylene with 16 quanta of total bend excitation have been assigned semiclassical quantum numbers in terms of the number of nodes along two families of periodic orbits. That is, we have associated with the eigenstates classical bending motions, which vary continuously between local bend and counter-rotation. The ability to semiclassically assign *all* of the quantum eigenstates in this way implies that there exists a very large degree of regularity in the quantum structure, which is surprising given that chaos dominates the classical phase space. This regularity in the quantum structure was previously undetected for two major reasons: First, identifying the regular nodal coordinates, if any, of quantum wave functions in a multidimensional (i.e., greater than two dimensions) space is a difficult task in general; this task is however made much easier by the identification of the important periodic orbits in the classical mechanics, which often form the "backbone" of the quantum structure. Second, there exist two families of quantum eigenstates, associated with the two major families of periodic orbits, and the energetic interleaving of these two families of states makes it difficult to identify regular progressions.

The semiclassical assignment of the quantum eigenstates in this paper, although by no means trivial, was made relatively easy by the reduction of the system to 2 degrees of freedom, which was accomplished by exploiting the existence of polyad quantum numbers, which are exactly conserved by the Hamiltonian model and approximately conserved (on the time scale of at least several picoseconds) by the real molecular system.[9] The semiclassical assignment scheme will of course become substantially more difficult in more dimensions. However, we believe that by projecting eigenstates onto various 2D axis systems defined by the important periodic orbits, it will be possible to perform similar analyses in higher dimensionality systems, although the analysis may by necessity be less detailed than that performed here. Indeed, the semiclassical approach will undoubtedly be of even greater importance for complicated, high-dimensionality systems.

Finally, we reiterate that the analysis that we have performed here has been based upon an *effective Hamiltonian* model, which is defined in terms of shift operators for the normal modes. Performing such an analysis using a potential energy surface would be much more difficult, due to the difficulties associated

with finding the needed action-angle variables analytically by solving the Hamilton-Jacobi equations. However, if a sufficiently accurate potential energy surface is available (this is not the case for acetylene), then two strategies are possible. First, an effective Hamiltonian can be fitted to the eigenspectrum that is computed from the potential surface.[24] Second, perturbation theory can be used to construct a (generally very high-order) effective Hamiltonian from the potential energy surface (three approaches are possible: canonical van Vleck perturbation theory[7] can be used to generate a quantum mechanical effective Hamiltonian, Gustavson perturbation theory[17] or the classical perturbation theories in refs 20−22, can be used to generate a classical action-angle Hamiltonian). One advantage of the perturbational approach, versus fitted effective Hamiltonians, is that exact (to a given order of perturbation theory) relations are obtained that relate the action-angle coordinates to a physical coordinate system for the molecule.

Lastly, there exist more sophisticated semiclassical quantization schemes that quantize even when tori are breaking down and under certain conditions in the chaotic region. A prime example of this is given in ref 28 and references therein. We have not needed these advanced tools in this analysis but we are sure that we will use them in the future.

References and Notes

(1) Plíva, J. *J. Mol. Spec.* **1982**, *44*, 165.

(2) Yamanouchi, K.; Ikeda, N.; Tsuchiya, S.; Jonas, D. M.; Lundberg, J. K.; Adamson, G. W.; Field, R. W. *J. Chem. Phys.* **1991**, *95*, 6330.

(3) Jonas, D. M.; Solina, S. A. B.; Rajaram, B.; Cohen, S. J.; Field, R. W.; Yamanouchi, K.; Tsuchiya, S. *J. Chem. Phys.* **1993**, *99*, 7350.

(4) Solina, S. A. B.; O'Brien, J. P.; Field, R. W.; Polik, W. F. *J. Phys. Chem.* **1996**, *100*, 7797.

(5) Rose, J. P.; Kellman, M. E. *J. Chem. Phys.* **1996**, *105*, 10743.

(6) McCoy, A. B.; Sibert, E. L., III *J. Chem. Phys.* **1996**, *105*, 459.

(7) Sibert, E. L., III; McCoy, A. B. *J. Chem. Phys.* **1996**, *105*, 469.

(8) Abbouti Temsamani, M.; Herman, M.; Solina, S. A. B.; O'Brien, J. P.; Field, R. W. *J. Chem. Phys.* **1996**, *105*, 11357.

(9) O'Brien, J. P.; Jacobson, M. P.; Sokol, J. J.; Coy, S. L.; Field, R. W. *J. Chem. Phys.* **1998**, *108*, 7100.

(10) Jacobson, M. P.; O'Brien, J. P.; Silbey, R. J.; Field, R. W. *J. Chem. Phys.* **1998**, *109*, 121.

(11) Jacobson, M. P.; Silbey, R. J.; Field, R. W. *J. Chem. Phys.* **1999**, *110*, 845.

(12) van Ede van der Pals, P.; Gaspard, P. *J. Chem. Phys.* **1999**, *110*, 5619.

(13) Jacobson, M. P.; Jung, C.; Taylor, H. S.; Field, R. W. *J. Chem. Phys.* **1999**, *111*, 600.

(14) Jacobson, M. P.; Field, R. W. *J. Phys. Chem. A* **2000**, *104*, 3073.

(15) Taylor, H. S.; Zakrzewski, J. *Phys. Rev. A* **1988**, *38*, 3732.

(16) Heller, E. J. *Phys. Rev. Lett.* **1984**, *53*, 1515.

(17) Joyeux, M.; Grebenshchikov, S. Y.; Schinke, R. *J. Chem. Phys.* **1998**, *109*, 8342.

(18) Keshavamurthy, S.; Ezra, G. S. *J. Chem. Phys.* **1997**, *107*, 156.

(19) Prosmiti, R.; Farantos, S. C. *J. Chem. Phys.* **1995**, *103*, 3299.

(20) Fried, L.; Ezra, G. S. *J. Comput. Phys.* **1987**, *8*, 397.

(21) Fried, L.; Ezra, G. S. *J. Chem. Phys.* **1987**, *86*, 6270.

(22) Fried, L.; Ezra, G. S. *Comput. Phys. Comm.* **1988**, *51*, 103.

(23) Goldstein, H. *Classical Mechanics*; 2nd ed.; Addison-Wesley: London, 1980.

(24) Jost, R.; Joyeux, M.; Skokov, S.; Bowman, J. *J. Chem. Phys.* **1999**, *111*, 6807.

(25) Ishikawa, H.; Field, R. W.; Farantos, S. C.; Joyeux, M.; Koput, J.; Beck, C.; Schinke, R. *Annu. Rev. Phys. Chem.* **1999**, *50*, 443.

(26) Beil, A.; Luckhaus, D.; Quack, M. *Ber. Bunsen-Ges. Phys. Chem.* **1996**, *100*, 1853.

(27) Beil, A.; Luckhaus, D.; Quack, M.; Stohner, J. *Ber. Bunsen-Ges. Phys. Chem.* **1997**, *101*, 311.

(28) Davis, M. J. *J. Chem. Phys.* **1997**, *107*, 106.